Materials Today Chemistry 24 (2022) 100909

Contents lists available at ScienceDirect

Materials Today Chemistry

journal homepage: www.journals.elsevier.com/materials-today-chemistry/

Loose nanofiltration membranes functionalized with in situ-synthesized metal organic framework for water treatment

S. Mohammad Nejad [a, f], S.F. Seyedpour [a, b, f], S. Aghapour Aktij [b, c, f], M. Dadashi Firouzjaei [d], M. Elliott [d], A. Tiraferri [e], M. Sadrzadeh [b, **], A. Rahimpour [b, *]

[a] Faculty of Chemical Engineering, Babol Noshirvani University of Technology, Shariati Ave., Babol, 47148-71167, Iran
[b] Department of Mechanical Engineering, 10-367 Donadeo Innovation Center for Engineering, Advanced Water Research Lab (AWRL), University of Alberta, Edmonton, AB, T6G 1H9, Canada
[c] Department of Chemical & Materials Engineering, 12-263 Donadeo Innovation Centre for Engineering, University of Alberta, Edmonton, AB, T6G 1H9, Canada
[d] Department of Civil, Construction and Environmental Engineering, University of Alabama, Tuscaloosa, 35487, USA
[e] Department of Environment, Land and Infrastructure Engineering (DIATI), Politecnico di Torino, Corso Duca Degli Abruzzi 24, 10129 Turin, Italy

ARTICLE INFO

Article history:
Received 6 January 2022
Received in revised form
16 March 2022
Accepted 20 March 2022
Available online 21 April 2022

Keywords:
Functionalized nanofiltration membranes
SBMA zwitterion
Metal organic frameworks
ZIF-7
Dye removal
Antifouling membranes

ABSTRACT

In this study, modified loose nanofiltration membranes were prepared by in-situ decoration with Zeolitic Imidazolate Framework-7 (ZIF-7) on the surface of porous polyethersulfone substrates functionalized with co-deposited sulfobetaine methacrylate (SBMA) zwitterion (ZW) and polydopamine (PDA). With the aid of ZW/PDA active layer co-deposition under mild conditions, ZIF-7 metal organic framework (MOF) nanocrystals were successfully formed and anchored onto the membrane surface via both non-covalent and covalent bonds to simultaneously achieve the desired selectivity and productivity of the loose nanofiltration membranes. The characterization results confirmed the successful deposition of the ZW/PDA active layer and the consequent decoration with ZIF-7 nanocrystals. The average water contact angle decreased notably from 81.4 to 51.43° upon the formation of ZIF-7. This membrane showed high rejection (~99.9%) of methyl blue and Congo red dyes and high water flux with dye solutions (around 40 L $m^{-2}h^{-1}$) at a very low applied pressure of 1.5 bar. Moreover, the filtration experiments revealed that functionalized membranes exhibited a significant reduction in fouling and biofouling propensity. Notably, the MOF-SBMA/PDA membrane displayed favorable antifouling behavior associated with a significant ability to recover flux upon simple physical cleaning. The combination of these two properties is possibly the most promising feature of the membrane proposed in this study.

1. Introduction

Dyes are toxic, carcinogenic, and teratogenic substances causing health problems, such as allergy, skin irritation, hard breathing, as well as kidney and liver dysfunction [1]. Dye contaminated wastewaters threaten human health and the environment [2] and must be properly treated before discharge into water streams or reuse. Nanofiltration (NF) is a promising solution due to its simple operation, high removal efficiency, and low operating costs and energy consumption [3–5]. However, fouling is still a severe challenge, resulting in reduced performance and membrane lifetime [6–8]. For this reason, one of the key ways to successfully deploy NF for wastewater treatment, recycling and reuse is to fabricate membranes with high permeation, rejection, and, importantly, low fouling tendency [9].

Regarded as a bio-inspired glue, PDA firmly attaches to any surface via in-situ self-polymerization of dopamine, forming a highly stable coating [10]. Furthermore, the catechol, quinone, and amine functional groups on the PDA layer offer secondary reaction sites for attaching other nanostructures and achieving further functionalization [11]. Membrane surfaces can thus inherit even higher antifouling properties by additional modification with compounds, such as zwitterions (ZWs) and metal-organic frameworks (MOFs) [12–15]. ZWs have shown superior antifouling

* Corresponding author.
** Corresponding author.
E-mail addresses: mohtada@ualberta.ca (M. Sadrzadeh), arahimpo@ualberta.ca (A. Rahimpour).
[f] These authors contributed equally to this work.

https://doi.org/10.1016/j.mtchem.2022.100909
2468-5194/

properties, particularly against protein and microorganisms [16–18]. The hydration layer formed by ZWs is typically dense, offering high surface hydrophilicity and consistent fouling control [6]. Among different types of zwitterionic materials, sulfobetaine methacrylate (SBMA) has attracted attention recently due to its easy polymerization [19]. Besides, SBMA is known for its excellent antifouling property in pressure-driven membrane processes [20]. Since SBMA has methacrylate functional groups, it can react with PDA amine groups via Michael addition [21].

In this way, the covalent grafting of the SBMA molecules to the PDA chains is facilitated under eco-friendly conditions. Taking into account the high solubility of ZWs in water, the introduction of ZWs into the PDA matrix leads to long-term stability during membranes operation. However, ZW structures cannot prevent microbial attachment and the biofilm buildup on membrane surfaces, ineffective in inactivating bacteria cells [22,23]. Furthermore, it has been reported that ZWs can act as nanoreactors for metal/metal nanoparticles and immobilize metal ions due to the presence of the negatively charged functional groups on their matrices [24,25]. The covalent bond between metal ions and ZWs facilitates the formation of highly stable MOFs on the membrane surface [26].

As a novel category of porous nanostructures, MOFs are an outstanding group of materials owing to their active centers, which are indeed the same or similar to those present in metal oxide NPs [14,27]. The main advantage of MOFs is their highly tunable structure by using diverse metal ions or the organic ligand [27]. As a class of MOFs, zeolitic imidazolate frameworks (ZIFs) have outstanding chemical stability and biocidal activity [28,29]. They also provide proper adsorption capacity for the removal of organic pollutants due to their high porosity (compared to those of activated carbon and clay), and the strong interactions between the pollutant molecules adsorbed onto ZIFs surfaces [30–32]. Considering the hydrophilic nature of both ZWs and ZIFs, their co-deposition with PDA is a practical method to develop multifunctional antifouling membranes [33].

Herein, we developed a method for PDA and sulfobetaine methacrylate (SBMA) co-deposition on porous PES supports under mild conditions. All membranes were comprehensively characterized, and their performance was evaluated under loose NF operating conditions to remove methyl blue (MB) and Congo red (CR) from aqueous solutions. The role of functional groups on the surface of PDA and ZWs in dye rejection, and the importance of PDA providing active sites for nucleation and growth of ZIF-7 were also investigated.

2. Materials and methods

2.1. Reagents

Polyethersulfone (PES, Ultrason E6020P, M_W = 58,000 g/mol) as polymer, N, N-dimethylformamide (DMF, 99.5%, Scharlau) as solvent, Triton X-100 (laboratory grade, Merck) and polyvinyl pyrrolidone (PVP, 99.5%, M_W = 25,000 g/mol, Merck) as pore formers were used for preparation of porous substrate casting solutions. Dopamine hydrochloride (DP, 98%, Merck), Trizma hydrochloride (Trizma-HCl, Merck), sulfobetaine methacrylate (SBMA, ≥ 98%, M_W = 279.36 g/mol, Merck), and phosphate-buffered saline (PBS) were purchased from Sigma Aldrich. $Zn(NO_3)_2.6H_2O$ (≥98.0%, Merck) and benzimidazole (≥98.0%, Merck) were used for the synthesis of ZIF-7 crystals. Methyl blue (MB, analytical grade, Merck) and Congo red (CR, analytical grade, Merck) were selected as model anionic dyes. Humic acid (technical grade) was purchased from Sigma-Aldrich and was used for antifouling assessment. Potassium dihydrogen phosphate (KH_2PO_4, 99.5%), glucose monohydrate, magnesium sulfate ($MgSO_4 \cdot 6H_2O$, 99%), sodium bicarbonate ($NaHCO_3$, 99.5%), calcium chloride ($CaCl_2$, 96%), and ammonium chloride (NH_4Cl, 99.5%), all purchased from Merck, were used for the preparation of the synthetic wastewater.

2.2. Fabrication of ZIF-7 functionalized NF membranes

The porous PES support membrane was fabricated via non-solvent induced phase inversion by immersion precipitation technique (denoted as blank membrane hereafter) [34]. The PDA self-polymerization on the membrane surface was performed by preparing 2.0 g/L DA in Tris (pH = 8.5, 0.089 M). The fixed blank membrane was soaked in DA solution with the active side facing the solution for 2 h at room temperature while shaking to provide sufficient oxygen for PDA formation. The PDA-coated membranes were thoroughly rinsed with deionized (DI) water and stored overnight in DI water to remove unattached monomers (denoted as PDA membrane). For the in-situ formation of ZIF-7, the PDA membrane was immersed in a metallic aqueous solution containing 0.446 g of $Zn(NO_3)_2 \cdot 6H_2O$ in 100 mL deionized water for 45 min [35,36]. After removing the excess metallic solution, the Zn anchored membrane was soaked in the benzimidazole solution containing 0.354 g in 100 mL of ethanol for 30 min at ambient temperature. Finally, this ZIF-7 functionalized membrane (denoted as MOF-PDA membrane) was washed with DI water and dried at room temperature. Both metallic and linker solutions were sonicated for 5 min before use to mitigate any aggregation.

To tailor the functionalization of ZIF-7, other membranes (labeled as MOF-SBMA/PDA) were obtained via co-deposition of PDA/SBMA on the PES support layer. Specifically, 1 g/L SBMA was incorporated into the 1 g/L DA solution, and all the steps mentioned above for the fabrication of the PDA membrane were repeated. Then, the SBMA/PDA coated membrane was subjected to the same sequential steps of ZIF-7 functionalization as the MOF-PDA membrane. Therefore, the membranes investigated in this study are included as: (i) blank membrane (PES porous support); (ii) PDA membrane; (iii) MOF-PDA membrane; and (iv) MOF-SBMA/PDA membrane. Fig. 1 illustrates the step-by-step procedures of membrane functionalization.

2.3. Membrane surface characterization

Field emission scanning electron microscopy (FE-SEM, MIRA3 TESCAN) coupled with an energy-dispersive X-ray Spectrometer (EDX) was used to characterize the membrane top surface and cross-sectional morphologies. The cross-section morphology of the blank and surface-modified membranes was further investigated by transmission electron microscopy (TEM, Philips/FEI Morgagni 268, The Netherlands), operated at 80 kV. Membrane coupons were initially stained with uranyl acetate and lead citrate and then embedded in Spurr's resin. Then, an ultramicrotome (Reichert-Jung Ultracut E, USA) was used to cut ultrathin sections of the membrane samples. Afterward, TEM operating at 80 kV was conducted to assess the obtained ultrathin sections mounted on a 300-mesh copper grid. Atomic force microscopy (AFM, Bruker Dimension Icon, USA) was applied to determine the surface roughness of membrane samples. To minimize the experimental error, the surface roughness was determined for three separate samples of each membrane type. Fourier transform infrared spectroscopy (FTIR, Thermo Scientific USA) was used to identify the functional groups of the anchored membrane. The surface electric potential of all membranes was evaluated with an Anton Paar SurPASS electrokinetic solid surface potential analyzer (Anton Paar USA, Ashland, VA). All the streaming potential measurements were conducted in a background electrolyte solution composed of 1 mM KCl at 25 °C, over a pH 4–9 range. The zeta potentials were calculated based on

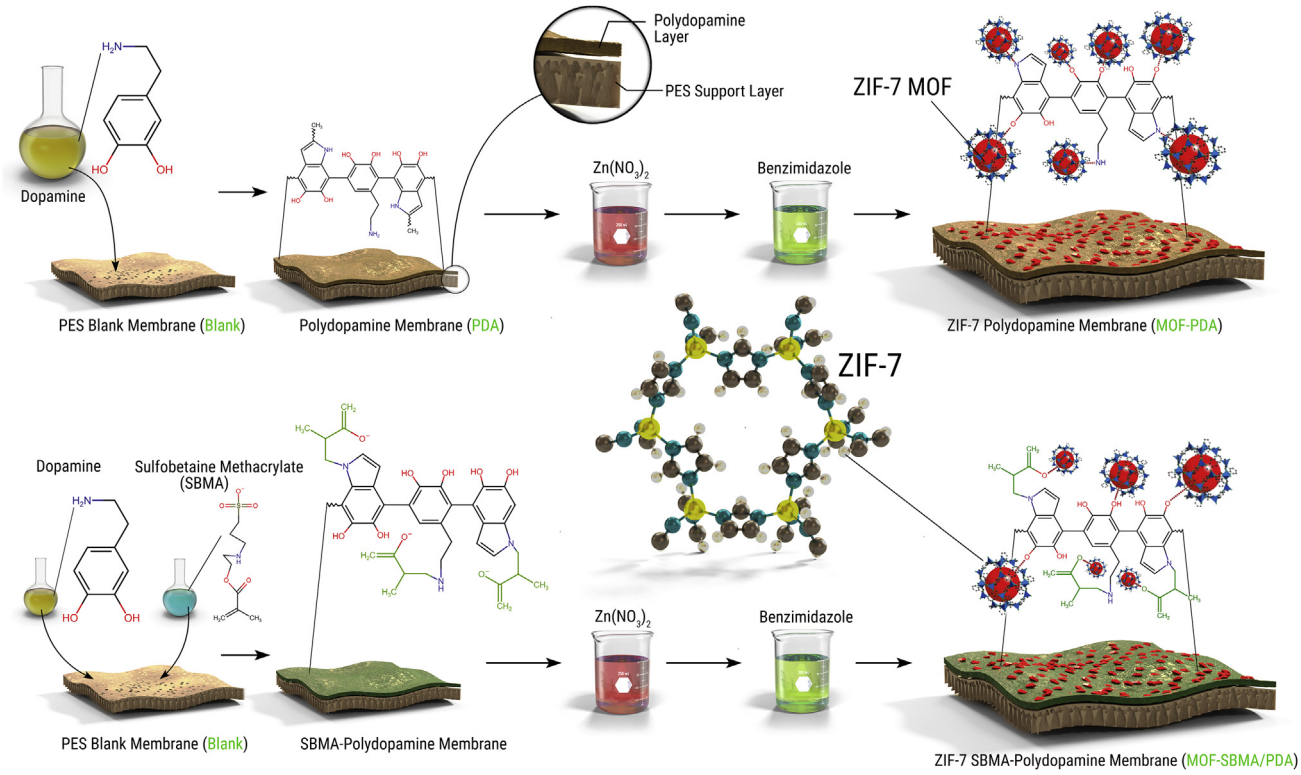

Fig. 1. Illustration of membrane functionalization procedures, including blank membrane; PDA coated membrane (PDA membrane); MOF deposition on PDA coated membrane (MOF-PDA membrane); MOFdeposition on SBMA/PDA coated membrane (MOF-SBMA/PDA membrane).

the Helmholtz-Smoluchowski equation. The zeta potential of two separate samples for each membrane type was measured to assess repeatability. The membrane surface hydrophilicity was evaluated through contact angle (CA) measurements (Dataphysics, OCA 15 plus), where an average value of five random positions was probed to calculate a meaningful average. The elemental composition and chemical features of the membrane surfaces were evaluated with X-ray photoelectron spectroscopy (XPS, Bestec, Germany).

2.4. Membrane transport and fouling evaluation

The flux and dye rejections of the membranes were evaluated at an operating pressure of 1.5 bar with a dead-end cell and with an effective membrane surface area of 30 cm^2. MB and CR were selected as model anionic dyes [37]. Further information on the dead-end setup and the performance evaluation are explained in **SI.1.1**. The organic fouling and bio-fouling propensity of the membranes were assessed with feed solutions containing humic acid and *E. coli* (model bacteria), respectively, guided by our previous studies (further detail on dynamic fouling experiments were provided in **SI.1.2**) [38].

2.5. Metal ion release rate

The release rate of zinc ions from the membranes was evaluated via batch experiments by coupled plasma-optical emission spectrometry (ICP-OES, Thermo Fisher iCAP6300 Duo, US). Briefly, MOF-PDA and MOF-SBMA/PDA membranes coupons (1 cm^2) were separately immersed in 60 mL of DI water and then placed on an orbital shaker (100 rpm) for several days and the water was replaced every 24 h. Aliquots were taken and acidified using HNO_3 and then analyzed by inductively coupled plasma optical emission spectrometry to determine their Zn content (further detail on Zn release was provided in **SI.1.3**).

3. Results and discussions

3.1. Physiochemical properties of the membranes

The catechol moiety of PDA can enhance the connection between the PES substrate and grafted SBMA or anchored ZIF-7. As illustrated in Fig. 1, a two-step surface modification took place for MOF-SBMA/PDA membranes. First, a thin layer of PDA and SMBA was initially co-deposited on the membrane surface, then ZIF-7 nanocrystals were in-situ attached to the active sites of this layer. Since SBMA has methacrylate functional groups, it would undergo an aza-Michael reaction with PDA amine groups. As a result, the nucleophilic amines of PDA can be connected to electron-withdrawing α, β-unsaturated carbonyl moieties [21]. Due to the presence of water molecules, hydrogen bonds are formed which can promote the aza-Michael reaction by increasing the electrophilic trait of carbon and the nucleophilic feature of the nitrogen atom in the amine (Figure SI.1). Co-deposition of SBMA/PDA is expected to facilitate post-modification of the membrane with ZIF-7 crystals and improve the stability of the coating. The dopamine monomers would act as bio-glue since their amine groups react with methacrylates moieties of SBMA to attain covalently grafting. Meanwhile, PDA is able to regulate the nucleation and growth sites, resulting in robust coordination interactions and, therefore, rapid bio-functionalization of ZIF-7 on the surface [39]. It is well established that the catechol groups on the PDA surface chelate various metal ions [40–44]. Eventually, the resulting Zn ions can serve as seeds that eventually grow into semi-spherical ZIF-7 nanostructures after introducing the benzimidazole ligand [45,46]. In

other words, the nucleated Zn ions is coordinated with the −NH functional moieties of benzimidazole ligand and formed stable ZIF-7 nanocrystal ZIF-7 on SBMA/PDA substrate [25,47,48].

The FTIR spectroscopy was conducted to distinguish the functional groups of the membrane surface and to confirm the successful deposition of PDA and ZIF-7 nanocrystal on the substrate (Fig. 2). Peaks appeared at around 1150 and 1240 cm^{-1}, corresponding to the symmetric O═S═O stretching vibration of the sulfone group and asymmetric C−O−C stretching vibration of the aryl ether group of the blank membrane, respectively [49]. The peaks observed at around 1300 and 1320 cm^{-1} can be assigned to the doublet from the asymmetric O═S═O stretching vibration [49]. The band at around 1485 cm^{-1} corresponds to the C−C stretching vibrations in the aromatic ring [50,51]. Furthermore, the absorption band observed at about 740 cm^{-1} is attributed to the out-of-plane C−H bending vibration of ortho-disubstituted benzene present in benzimidazole ligand of the ZIF-7, which is in accordance with previously reported studies [52]. Comparing the spectra of all membranes, a new peak emerged at 775 cm^{-1} for MOF-PDA and MOF-SBMA/PDA membranes, which corresponds to the ZIF-7, corroborating the formation of the ZIF-7 nanocrystals on the membranes surface [53]. The benzimidazole ligand displayed several N−H signals between 3300 and 2500 cm^{-1} (Aldrich Library of FTIR spectra, ed II, vol. 3). However, many of these peaks disappeared after the coordination with Zn atoms that implies the formation of ZIF-7 [54,55]. The stretching vibrations of MOF-PDA and MOF-SBMA/PDA membranes at around 916 cm^{-1} can be ascribed to the Zn−OH bond, confirming the decoration of Zn atoms on the catechol groups of PDA [56,57]. Meanwhile, a peak at around 975 cm^{-1} is attributed to the C−N stretching vibration of the ZIF-7 structure [28].

The elemental composition and chemical structure of blank and modified membranes were evaluated by XPS analysis and the results are shown in Fig. 3. The survey spectra of all membranes mainly comprise the energy peaks of carbon (C), nitrogen (N), oxygen (O), and sulfur (S) atoms, located at 284.5, 399, 532, and 168.6 eV, respectively. However, the appearance of two new Zn signals located at 1021.3 and 1044.4 eV (attributed to Zn $2p_{3/2}$ and $2p_{1/2}$, respectively) indicateed the presence of ZIF-7 nanocrystals on the surface of both ZIF-7 decorated membranes (MOF-PDA and MOF-SBMA/PDA) [58,59]. The elemental compositions of blank and modified membranes are presented in Table 1. N atoms on the blank membrane are attributed to the presence of PVP in the support layer. After PDA deposition, the content of N atoms decreased slightly and then increased significantly after ZIF-7 decoration [60]. The negligible reduction of N and slight increment of S atoms in MOF-SBMA/PDA membrane indicated the incorporation of SBMA to the PDA structure.

Further information on the chemical structure of membranes and coordination of the ZIF-7 nanocrystals was obtained by the deconvolution of the C1s and N1s high-resolution spectra (Figure SI.2). Regarding the blank membrane containing PVP as an additive, the deconvoluted spectrum of C 1s reveals C═C/C−C, C−N/C−O, C−S, and O═C−N bonds located at binding energies of 284.5, 285.9, and 287.4, and 288.2 eV, respectively [59]. Due to the presence of PVP, the de-convoluted N 1s spectrum represents the −NH− and N^{+} bonds at 400.6 and 401.9 eV. The de-convoluted C 1s spectrum of PDA and MOF-PDA membranes showed three main peaks, including C−C/C−H, C−N/C−O, and C═O bonds located at binding energies of 284.5, 285.7, and 287.1 eV, respectively [39,61]. Besides, the de-convoluted N 1s spectrum of PDA coated membrane showed the ═N−C, C−N−C, and N−C bonds at 398.8, 399.9, and 400.7 eV, respectively. The deconvoluted C 1s spectrum of MOF-SBMA/PDA membrane revealed C−C/C−H, C−N, C−O/C−S, and C═O/C═N bonds located at binding energies of 284.5, 285.7, and 287.3 eV, and 287.9 eV, respectively [59]. For both ZIF-7 modified

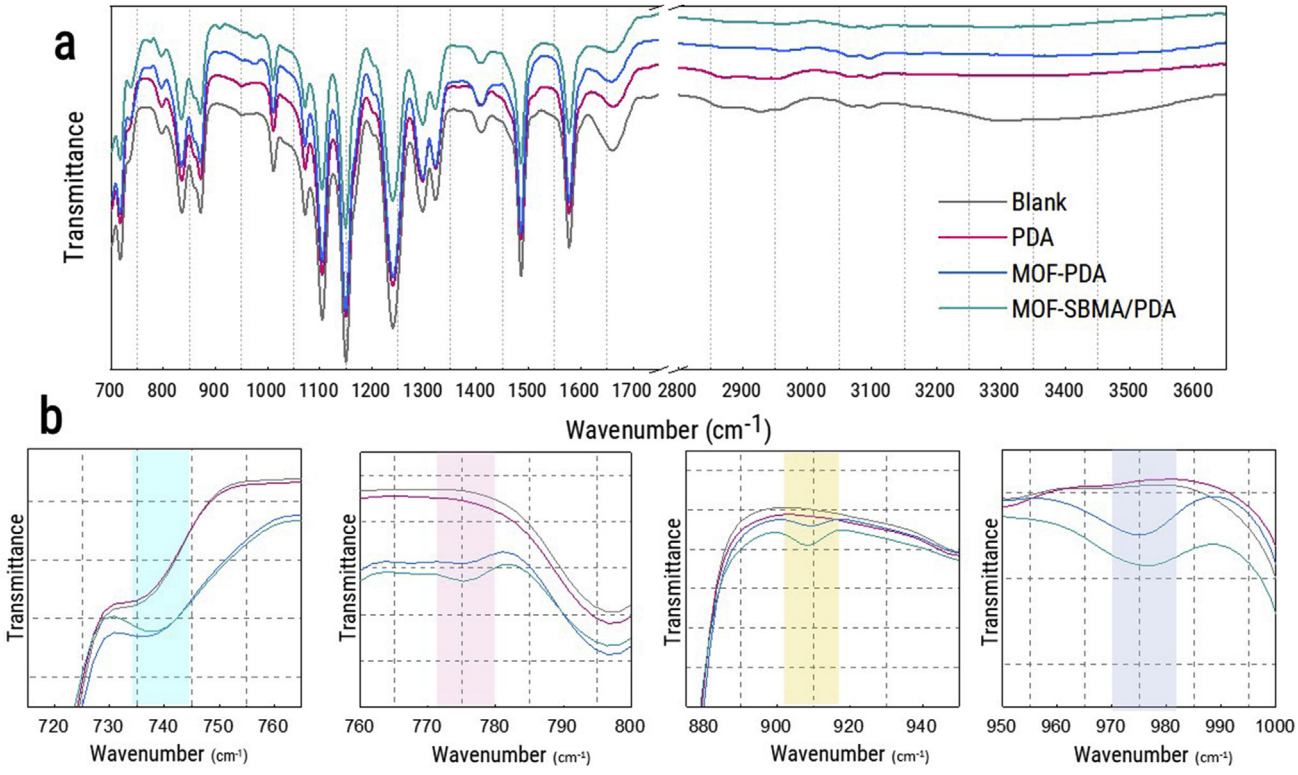

Fig. 2. FITR spectra of blank and modified membranes: (a) survey and (b) high-resolution spectra.

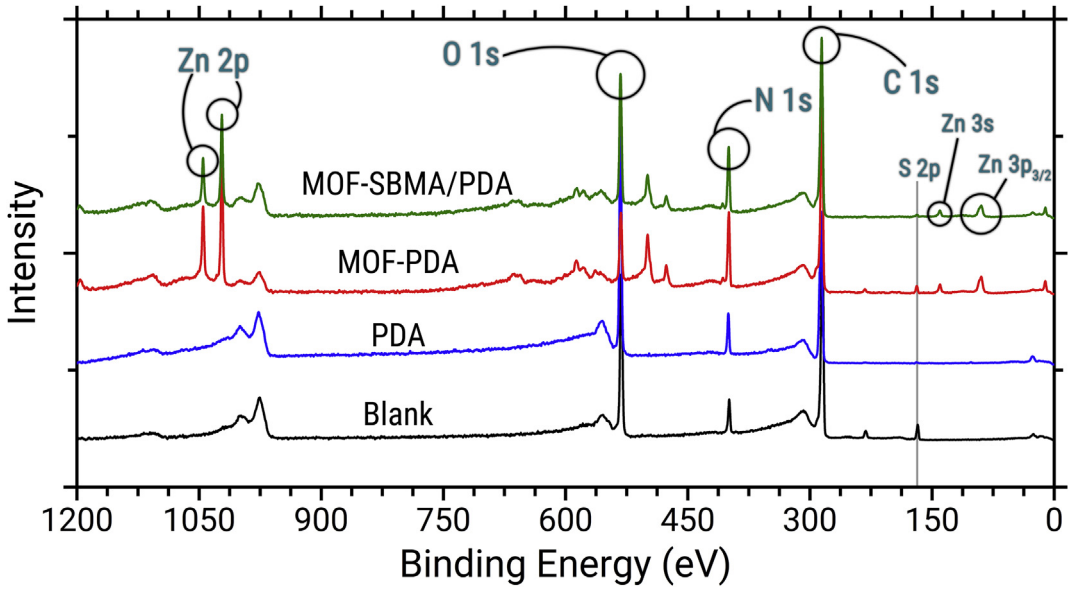

Fig. 3. The XPS survey spectra of blank and modified membranes.

membranes, owing to the presence of benzimidazole ligand, three kinds of N-containing functional groups can be observed in the deconvoluted spectrum of N1s [62]. These include pyridinic (=N– bond), pyrrolic (–NH– bond), and quaternary N centers, located at 398.5, 399, and 400.4 eV, respectively [55,63]. After reacting with Zn atoms, a signal appeared that may be associated with the protonated N atoms coordinated with Zn [63,64]. Considering all this information, it can be concluded that SBMA/PDA layer was successfully deposited on the PES surface and ZIF-7 nanocrystal formed on functional groups.

The surface and cross-sectional morphologies of all membranes were assessed by FE-SEM and TEM (Fig. 4). SEM micrographs showed relatively smooth surfaces for the PDA membrane, while all the ZIF-7 decorated membranes had a rougher surface, comprising some PDA aggregates and ZIF-7 nanocrystals on the surface. PDA catechol functional groups can provide anchor sites to react with positively charged Zn ions of ZIF-7 nanocrystals. Hence, some semi-spherical ZIF-7 nanocrystals were formed on the surface of MOF-PDA and MOF-SBMA/PDA membranes (Figure SI.3) [46]. Compared to the MOF-PDA membrane, the quantity of ZIF-7 increased significantly on the MOF-SBMA/PDA membrane.

A thicker active layer was observed on the surface of PDA-coated membranes, together with a denser upper portion of the support, compared to the blank membrane (Fig. 4 f-h). Other than forming a surface PDA layer, it is likely that dopamine monomers penetrated the membrane and partly blocked the pores upon polymerization [65]. The SEM micrographs (Fig. 4g vs. 4h) suggested that the clogging degree of the MOF-SBMA/PDA membrane was higher than PDA and MOF-PDA membranes. This phenomenon is likely due to the co-deposition of PDA/SBMA, which would produce a denser structure as chain entanglement occurs. When a denser structure forms on the surface, it also provides more active sites and functional groups for further functionalization, thereby allowing a larger quantity of ZIF-7 nanocrystals to form on the surface, as indicated by the SEM micrographs (Fig. 4c vs. 4d).

The corresponding EDX mapping (Figure SI.4) of ZIF-7 decorated membranes revealed the presence of Zn ions and nitrogen atoms on the surface. The content of Zn increased on the MOF-SBMA/PDA membrane compared to MOF-PDA, consistent with SEM images. In addition, TEM images (Fig. 4i–l and Figure SI.5) illustrated that the surface of the blank membrane was successfully modified as ZIF-7 nanocrystals formed on the MOF-PDA and MOF-SBMA/PDA surfaces due to accessibility to more functional groups on the surface.

AFM images of membrane surfaces and their relevant roughness parameters are illustrated in Fig. 5a–d and Table 2, respectively. The average roughness of the membrane decreased from 45.32 to 28.81 nm after PDA deposition, indicating appropriate surface coverage. The surface roughness of the MOF-PDA membrane increased to 39.59 nm due to the formation of some ZIF-7 nanocrystals on the surface of the PDA membrane. However, the MOF-SBMA/PDA membrane demonstrated the roughest surface among all membranes as the density and quantity of decorated ZIF-7 nanocrystals increased, consistent with both TEM and FE-SEM results. Even though it is generally accepted that a rougher membrane is more inclined to fouling, especially biofouling, the overall fouling tendency is governed by a complex interplay between surface morphology, chemistry, charge, and wettability [66].

The CA analysis was carried out to evaluate the surface hydrophilicity of the blank and modified membranes, and the results are depicted in Fig. 5e. The average CA declined noticeably from 81.4° for the blank membrane to 71.4°, 56.6°, and 51.43 for PDA, MOF-PDA, MOF-SBMA/PDA membranes, respectively. This descending trend suggests enhanced surface wettability and higher affinity to water molecules. The hydrophilic functional groups of PDA, as well as the sulfonate terminals on the SBMA structure (in the case of MOF-SBMA/PDA membrane), could significantly increase the hydrophilicity of modified membranes. Such an enhancement in surface hydrophilicity is expected to hinder foulant attachment and therefore fouling propensity [67–70], due to the formation of a thin boundary layer of water on the hydrophilic surface [71].

Table 1
Elemental compositions of blank and modified membranes.

Membrane	Atomic concentration (%)				
	C(1s)	O(1s)	N(1s)	Zn(2p)	S(2p)
Blank	60.2	30.30	6.80	–	2.70
PDA	69.9	22.00	5.90	–	2.20
MOF-PDA	70.90	9.30	13.20	5.50	1.10
MOF-SBMA/PDA	66.50	16.90	12.00	3.30	1.30

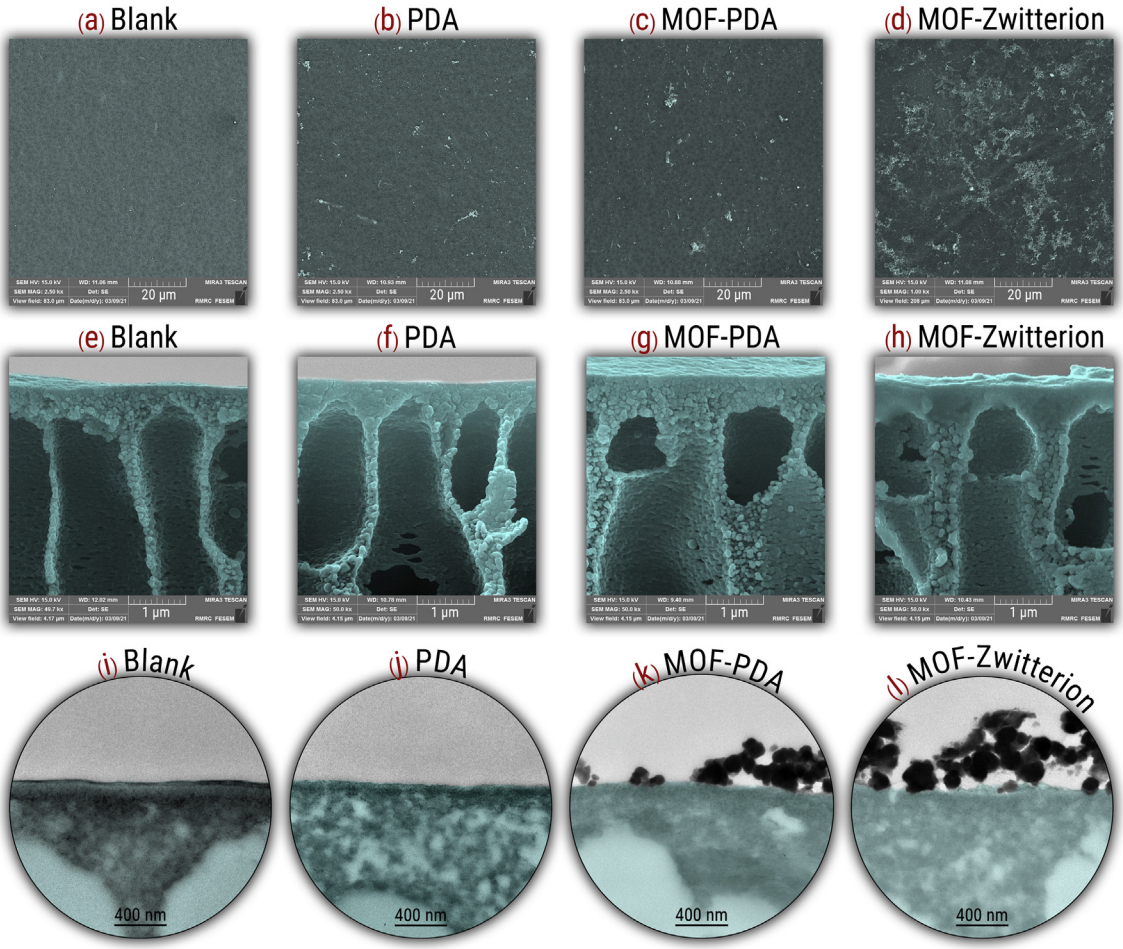

Fig. 4. (a–d) The surface FE-SEM images, (e–h) the cross-sectional FE-SEM images, and (i–l) TEM images of the blank and modified membranes.

When a feed solution contains charged foulants, surface charge also plays an essential role in reducing the fouling tendency [72–74]. As illustrated in Fig. 5f, all membranes demonstrated negative zeta potential over the pH range 4–9. As expected, the zeta potential of all membranes became more negative by increasing the pH, suggesting the presence of various moieties undergoing acid-base reactions with pH. The MOF-SBMA/PDA membrane showed the lowest surface charge at acidic pH and thus the lowest isoelectric potential. It also provided the minimum change in zeta potential over the pH range. On the other hand, the

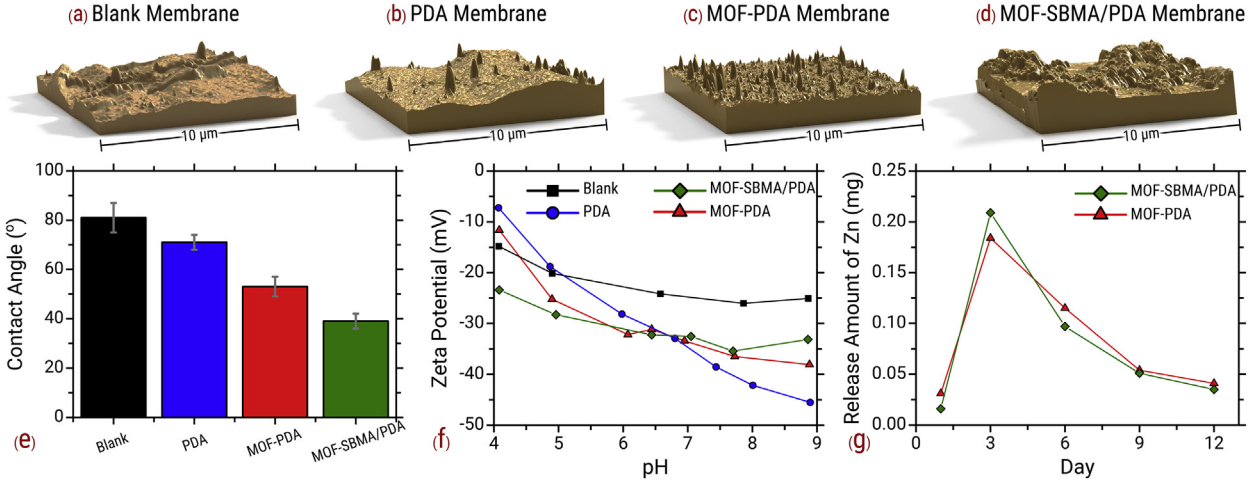

Fig. 5. (a–d) Surface AFM images, (e) contact angle, (f) zeta potential of the blank and modified membranes, and (g) release rate of the MOF-PDA and MOF-SBMA/PDA modified membranes.

Table 2
Roughness parameters of membranes.

Membrane type	Roughness parameters (nm)	
	Average roughness (R_a)	Root mean squared roughness (R_{rms})
Blank PES	45.32	58.37
PDA	28.81	38.18
MOF-PDA	39.59	52.65
MOF-SBMA/PDA	238.50	291.50

PDA membrane had the highest IEP, a steeper potential curve as a function of pH, and the greatest negative charge among all membranes at basic pH values. This implies that MOF-SBMA/PDA, with a bulkier molecular structure, contains less ionizable functional groups, such as hydroxyl (OH^-), carboxyl ($R—COO^-$), and amine ($R—NH_3^+$), than the PDA. This result indicates the significant effect of dopamine functional groups, protonating and deprotonating at different pH values, on the surface charge of membranes [75–77]. MOF-PDA membranes showed an intermediate behavior between PDA and MOF-SBMA/PDA membranes, consistent with their surface nature. Generally, a membrane with a negative surface charge is less prone to bacterial deposition and hence biofouling in normal pH ranges [78], as bacterial cells carry negative charges in the pH range of 4–9 [79,80].

Since the stability of decorated ZIF-7 and the controlled release of zinc ions would considerably affect the performance and anti-biofouling properties of the modified membranes, zinc leakage assessment was conducted. As displayed in Fig. 5g, both MOF-PDA and MOF-SBMA/PDA membranes demonstrated the same release trend of zinc ions, which included a rapid increasing rate for the first 3 days, followed by a gradual decrease in the subsequent 3-day periods. The initial relatively high zinc release may be ascribed to the release of loosely bound zinc from the surface. In the case of the MOF-SBMA/PDA membranes, the observed slightly higher release rate is rationalized with the higher density of deposited ZIF-7. The total leakage rate of zinc ion was low in both membranes and reached a negligible level at the end of the assessing process [15,34].

3.2. Filtration performance and fouling evaluation of membranes

The separation performance of blank and modified membranes in terms of water flux and dye rejection is presented in Fig. 6. The MOF-PDA membrane's water flux was significantly lower than that of the PDA membrane. The water flux decreased from 78.6 to 28.3 and from 75.3 to 25.6 LMH for CR and MB solutions, respectively. According to the permeability-selectivity trade-off, the dye removal rate by the MOF-PDA membrane increased from 52 to 94% for CR and from 55 to 96% for MB. This behavior indicates the formation of effective selective layer on the membrane surface via PDA deposition followed by the decoration of ZIF-7 nanocrystals [48]. Although the formation of ZIF-7 nanocrystals on the PDA layer slightly sacrificed membrane flux, it significantly improved dye rejection.

Interestingly, the water flux of the MOF-SBMA/PDA membrane was notably higher than that observed with the membrane that did not contain zwitterions (MOF-PDA), with an increment from 28.3 LMH to 41.5 LMH for the CR solution. At the same time, the rejection performance of this membrane also increased remarkably up to 99.9% for both dyes, attributed to the formation of a denser selective layer, as supported by SEM and TEM images. A possible explanation can be the improvement in membrane hydrophilicity by adding SBMA. SBMA can slow down the PDA polymerization via Michael addition, resulting in a more hydrophilic surface, facilitating water molecules transport (Fig. 5e) [48,68].

"It is worth noting that the mass transfer resistance introduced by selective layer is of crucial importance for membrane separation since permeability is inversely proportional to the thickness of this layer. As indicated in FE-SEM and TEM images, a slight surface coverage happens in the case of PDA deposition, whereby an ultrathin coverage layer with subtle change is observed after the PDA deposition on the PES surface. However, the thickness of this layer can be increased with the surface decoration of ZIF-7 or the introduction of SBMA ZW structures. Therefore, two parameters should be considered when comparing the flux of surface-modified membranes: (i) increased hydrophilicity and (ii) mass transfer resistance. A trade-off between these two parameters controls the water flux. The mass transfer resistance of the MOF-SBMA membrane is higher than that of the PDA one, resulting in flux decline. Nevertheless, as confirmed by contact angle measurement, the surface hydrophilicity of MOF-SBMA/PDA membrane enhanced after the introduction of ZW to the PDA matrix, and this resulted in water flux increment compared to that of the MOF-PDA one, providing facilitated transport of water molecules."

The functional groups present on the PDA chain and SBMA structure may improve dye rejection owing to the surface charge adjustment by multiple interactions [81]. In fact, some hydrogen bond, electrostatic, and π-π interactions with dye molecules can be formed due to the existence of amine, imine, and catechol moieties on the PDA chain that can increase the selective adsorption performance of the outmost layer [82,83]. It remains to be determined whether this high performance can be maintained for long-term filtrations.

Fig. 7 illustrates the results of both organic and biofouling assessments of PDA, MOF-PDA, and MOF-SBMA/PDA membranes and their corresponding flux recovery ratios. The flux declined

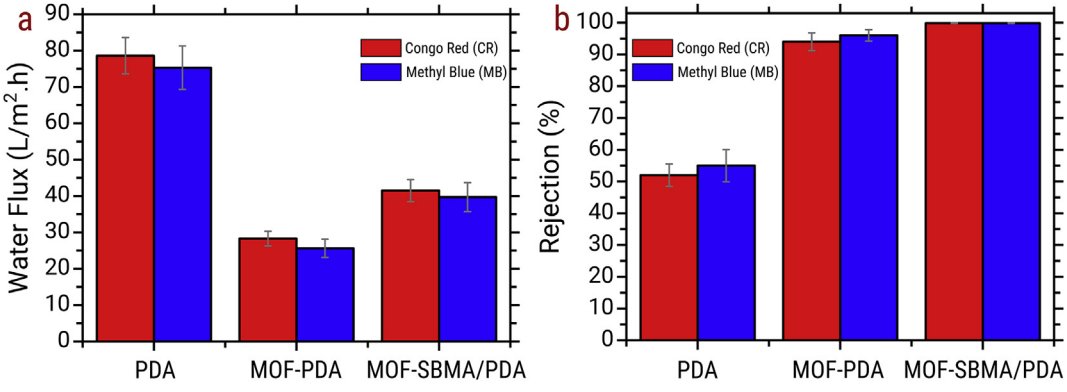

Fig. 6. (a) Water flux and (b) dye rejection of blank and modified membranes (ΔP = 1.5 bar).

sharply in the first phase of all fouling experiments, and this phenomenon was more severe for the PDA membrane. The results in Fig. 7a indicated a lower flux decline rate for the MOF-SBMA/PDA in the presence of humic acid. Moreover, as illustrated in Fig. 7b, after a simple water washing process conducted for 30 min, flux recovery ratios (FRR) of 16.8, 40.4, and 60.3% were achieved for PDA, MOF-PDA, and MOF-SBMA/PDA membranes, respectively. The antifouling property of the MOF-SBMA/PDA membrane is attributed to the weaker adhesion of humic acid molecules to the hydrophilic surface of this membrane [84]. Furthermore, the nitrogen and oxygen atoms of ZIF-7 nanocrystals can also attract water molecules and form a hydration layer that mitigates the humic acid deposition [85].

The results of biofouling experiments are illustrated in Fig. 7c. The water flux of the PDA membrane declined after the introduction of *E. coli* to the feed solution, while the antifouling tendency of modified MOF-PDA and MOF-SBMA/PDA membranes improved significantly upon ZIF-7 formation and/or SBMA co-deposition. In addition, after physical cleaning (Figs. 7d), 9.7 and 37.9, and 47% FRR were attained for PDA, MOF-PDA, MOF-SBMA/PDA membranes, respectively. These FRR values are consistent with the antibacterial activity of ZIF-7 nanocrystals, which hinder biofilm formation. SBMA molecules tend to prevent microbial attachment on membrane surfaces, but they are unsuccessful in inactivating bacteria cells [22,23]. Therefore, integrating passive anti-adhesion (SBMA) and active antibacterial (ZIF-7) strategies can result in synergistic effects [8,24,86]. In addition, the protonated amine groups possibly trigger additional antibacterial properties, as they can result in cell lysis when in contact with the bacteria [87,88].

In order to also elucidate the effect of the dye on fouling, the flux decline was investigated in the presence of CR for ~24 h (Fig. 7e), which again revealed the lower fouling tendency for both MOF

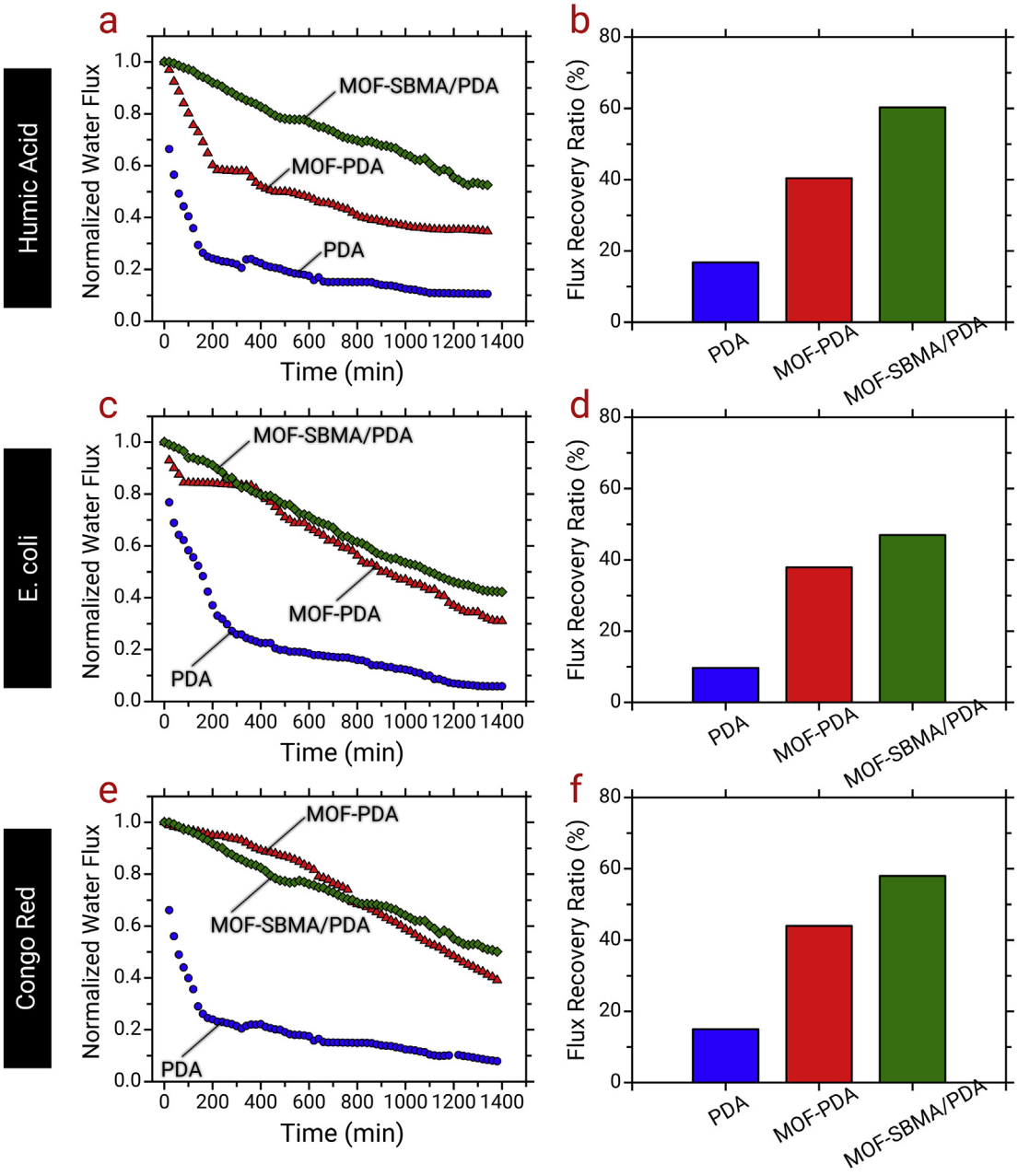

Fig. 7. Long-term antifouling performance of the PDA, MMOF-PDA, and MOF-SBMA/PDA membranes versus time.

Table 3
A comparison of the performance of various surface-modified membranes developed for dye removal reported in the literature.

Membrane type	Membrane Support layer	Dye type	Dye Carbon number	Modifying agent	Modifying technique	Applied pressure	Permeability ($L/m^2.hr.bar$)	Dye removal (%)	Ref
NF	PSF	Anionic (MB)	37	TEOA-TMC-PAA	Interfacial polymerization and physiochemical	5 bar	8.05	99.6	[89]
TFN	HPAN	Anionic (CR, MB, reactive black5, Direct red 23)	32 37 26 35	PVP-uio-66-NH_2-PVA-GA	Drop coating	4 bar	13.09	99.89–100	[90]
NF	HPAN	Anionic (CR, MB) Cationic(MB)	32 37 16	Sulfonated Dopamine(SDA)	Interfacial polymerization	6 bar	10.36	99.9	[91]
Composite	PES	Anionic(Reactive black 5, Reactive Green 19)	26 40	MOS_2-PSBMA	MMM(Phase inversion)	6 bar	18.05	98.2 99.3	[92]
Loose NF	HPAN	Anionic(CR, MB)	32 37	PEI-GA	Dip Coating	2 bar	25.50	97.1 97.3	[62]
Loose NF	PVDF	Anionic(CR)	32	PAA	UV-grafting	4 bar	26	99.38	[93]
Composite	PAN	Anionic (CR, Reactive-black-5, reactive orange16	32 26 20	PDA-PEI/TiO_2 -Ag	Coating and vacuum filtration	2 bar	40.6	99.6 99.5 96.2	[94]
Loose NF	PES	Anionic (CR) Anionic (MB)	32 37	MOF-SBMA/PDA	Coating and surface functionalization	1.5 bar	28	99.9	This work

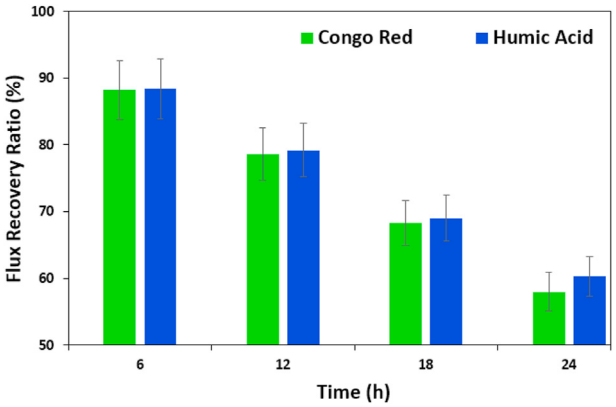

Fig. 8. Flux recovery ratio for the MOF-SBMA/PDA membrane over several fouling and cleaning sequences. The cycle fouling and washing experiment was conducted under the same condition applied for the long-term fouling, simple water washing for 30 min was applied with no chemical cleaning and flux was recorded afterward.

modified membranes compared to PDA membrane. FRR values of 15, 44, and 58% were achieved for PDA, MOF-PDA, and MOF-SBMA/PDA membranes, respectively (Fig. 7f). The remarkable antifouling properties of both MOF-PDA and MOF-SBMA/PDA can be primarily attributed to their enhanced hydrophilicity and highly negative surface charge.

Table 3 presents a comparison between the best performing membrane in this study, namely, MOF-SBMA/PDA, and some membranes developed for dye removal reported in the literature. The productivity (water flux normalized by applied pressure) and separation performance of the MOF-SBMA/PDA membrane are among the highest ones in the literature. Notably, the MOF-SBMA/PDA membrane displayed favorable antifouling behavior associated with a significant ability to recover flux upon simple physical cleaning. The combination of these two properties is possibly the most promising feature of the membrane proposed in this study.

Furthermore, a typical cycle flux recovery of MOF-SBMA/PDA membrane over several fouling and cleaning sequences is presented in Fig. 8. As can be seen, in the case of CR and humic acid fouling experiments, the membrane flux reduced over time, and the flux recovery ratio declined from 88.2% to 58% for CR from the first to the final cycle. The same trend was observed for the humic acid fouling experiment, and the water flux recovery ratio decreased from 88.4% to 60.3% over 24 h. The flux recovery ratio reduced up to 35% during four cycles compared to the initial fouling phase. In addition, after four cycles of fouling tests, the final rejection of 94.1% and 99.4% were obtained for the MOF-PDA and MOF-SBMA/PDA membranes.

4. Conclusion

In this study, simple in-situ heterogeneous nucleation and growth of ZIF-7 nanocrystals were conducted on the functional sites of PDA-coated membranes. This ecofriendly procedure was also adopted for the co-deposition of SBMA zwitterion with PDA through the aza-Michael reaction to obtain a dense layer with high dye rejection capability. The findings represent increased grafting density and hence higher active sites for ZIF-7 deposition, as the quantity and thickness of ZIF-7 nanocrystals enhanced considering the TEM and FE-EM images. Meanwhile, the incorporation of SBMA into the PDA matrix played a favorable role in improving the performance of the resultant membrane. The results indicated that MOF-SBMA/PDA membrane provided suitable water flux (~41 LMH at 1.5 bar) and high dye retention for loose nanofiltration applications (~99.9% for MB and CR dyes). More importantly, the membrane demonstrated remarkable antifouling properties due to the synergetic presence of hydrophilic ZIF-7 nanocrystals and SBMA zwitterion over a long-term fouling experiment and the final CR rejection of 94.1% and 99.4% were observed for the MOF-PDA and MOF-SBMA/PDA membranes after four cycles of fouling tests. Owing to simplicity, the proposed functionalization strategy in this paper offers a platform for developing diverse surface-modified membranes with promising potential for industrial applications that require the separation of low molecular weight compounds from aqueous streams.

Credit author statement

Sina Mohammad Nejad: Conceptualization, Investigation, Methodology, Writing – original draft, **S. Fatemeh Seyedpour:** Conceptualization, Investigation, Methodology, Writing – original draft, Writing – review & editing, **Sadegh Aghapour Aktij:** Conceptualization, Investigation, Methodology,; Data curation; Formal **Mostafa Dadashi Firouzjaei:** Conceptualization, Formal

analysis, Investigation, Methodology, Validation **Mark Elliott:** Project administration, Resources, Supervision, Writing – review & editing **Alberto Tiraferri:** Investigation, Methodology, Project administration, Supervision, Writing – review & editing **Mohtada Sadrzadeh**: Funding acquisition, Investigation, Methodology, Supervision, Writing – review & editing **Ahmad Rahimpour:** Funding acquisition, Investigation, Project administration, Resources, Supervision, Writing – review & editing.

Declaration of competing interest

The authors declare that they have no known competing financial interests or personal relationships that could have appeared to influence the work reported in this paper.

Acknowledgment

The authors gratefully acknowledge the financial support provided by the Natural Sciences and Engineering Research Council of Canada (NSERC), Alberta Innovates, and Canada's Oil Sands Innovation Alliance (COSIA).

Appendix A. Supplementary data

Supplementary data to this article can be found online at https://doi.org/10.1016/j.mtchem.2022.100909.

References

[1] M.D. Firouzjaei, F.A. Afkhami, M.R. Esfahani, C.H. Turner, S. Nejati, Experimental and molecular dynamics study on dye removal from water by a graphene oxide-copper-metal organic framework nanocomposite, J. Water Proc. Eng. 34 (2020) 101180.
[2] B.J. Quah, H.S. Warren, C.R. Parish, Monitoring lymphocyte proliferation in vitro and in vivo with the intracellular fluorescent dye carboxyfluorescein diacetate succinimidyl ester, Nat. Protoc. 2 (9) (2007) 2049–2056.
[3] R. Zhang, Y. Liu, M. He, Y. Su, X. Zhao, M. Elimelech, Z. Jiang, Antifouling membranes for sustainable water purification: strategies and mechanisms, Chem. Soc. Rev. 45 (21) (2016) 5888–5924.
[4] A. Asad, S.A. Aktij, P. Karami, D. Sameoto, M. Sadrzadeh, Micropatterned thin-film composite poly (piperazine-amide) nanofiltration membranes for wastewater treatment, ACS Applied Polymer Materials 3 (12) (2021) 6653–6665.
[5] S.A. Aktij, A. Rahimpour, A. Figoli, Low content nano-polyrhodanine modified polysulfone membranes with superior properties and their performance for wastewater treatment, Environ. Sci.: Nano 4 (10) (2017) 2043–2054.
[6] M.D. Firouzjaei, S.F. Seyedpour, S.A. Aktij, M. Giagnorio, N. Bazrafshan, A. Mollahosseini, F. Samadi, S. Ahmadalipour, F.D. Firouzjaei, M.R. Esfahani, Recent advances in functionalized polymer membranes for biofouling control and mitigation in forward osmosis, J. Membr. Sci. 596 (2020) 117604.
[7] M. Dadashi Firouzjaei, M. Pejman, M.S. Gh, S.A. Aktij, E. Zolghadr, A. Rahimpour, M. Sadrzadeh, A.A. Shamsabadi, A. Tiraferri, M. Elliott, Functionalized polyamide membranes yield suppression of biofilm and planktonic bacteria while retaining flux and selectivity, Separ. Purif. Technol. 282 (2022) 119981.
[8] P. Karami, S.A. Aktij, B. Khorshidi, M.D. Firouzjaei, A. Asad, M. Elliott, A. Rahimpour, J.B. Soares, M. Sadrzadeh, Nanodiamond-decorated thin film composite membranes with antifouling and antibacterial properties, Desalination 522 (2022) 115436.
[9] M.R. Esfahani, S.A. Aktij, Z. Dabaghian, M.D. Firouzjaei, A. Rahimpour, J. Eke, I.C. Escobar, M. Abolhassani, L.F. Greenlee, A.R. Esfahani, Nanocomposite membranes for water separation and purification: fabrication, modification, and applications, Separ. Purif. Technol. 213 (2019) 465–499.
[10] H.W. Kim, B.D. McCloskey, T.H. Choi, C. Lee, M.-J. Kim, B.D. Freeman, H.B. Park, Oxygen concentration control of dopamine-induced high uniformity surface coating chemistry, ACS Appl. Mater. Interfaces 5 (2) (2013) 233–238.
[11] Q. Ye, F. Zhou, W. Liu, Bioinspired catecholic chemistry for surface modification, Chem. Soc. Rev. 40 (7) (2011) 4244–4258.
[12] D.K. Yeon, S. Ko, S. Jeong, S.-P. Hong, S.M. Kang, W.K. Cho, Oxidation-mediated, zwitterionic polydopamine coatings for marine antifouling applications, Langmuir 35 (5) (2018) 1227–1234.
[13] Z. Wang, Z. Wang, S. Lin, H. Jin, S. Gao, Y. Zhu, J. Jin, Nanoparticle-templated nanofiltration membranes for ultrahigh performance desalination, Nat. Commun. 9 (1) (2018) 1–9.
[14] M. Pejman, M. Dadashi Firouzjaei, S. Aghapour Aktij, E. Zolghadr, P. Das, M. Elliott, M. Sadrzadeh, M. Sangermano, A. Rahimpour, A. Tiraferri, Effective strategy for UV-mediated grafting of biocidal Ag-MOFs on polymeric membranes aimed at enhanced water ultrafiltration, Chem. Eng. J. 426 (2021) 130704.
[15] M.D. Firouzjaei, A.A. Shamsabadi, S.A. Aktij, S.F. Seyedpour, M. Sharifian Gh, A. Rahimpour, M.R. Esfahani, M. Ulbricht, M. Soroush, Exploiting synergetic effects of graphene oxide and a silver-based metal–organic framework to enhance antifouling and anti-biofouling properties of thin-film nanocomposite membranes, ACS Appl. Mater. Interfaces 10 (49) (2018) 42967–42978.
[16] M. Pejman, M.D. Firouzjaei, S.A. Aktij, P. Das, E. Zolghadr, H. Jafarian, A.A. Shamsabadi, M. Elliott, M.R. Esfahani, M. Sangermano, M. Sadrzadeh, E.K. Wujcik, A. Rahimpour, A. Tiraferri, Improved antifouling and antibacterial properties of forward osmosis membranes through surface modification with zwitterions and silver-based metal organic frameworks, J. Membr. Sci. 611 (2020) 118352.
[17] M. Pejman, M. Dadashi Firouzjaei, S. Aghapour Aktij, P. Das, E. Zolghadr, H. Jafarian, A. Arabi Shamsabadi, M. Elliott, M. Sadrzadeh, M. Sangermano, A. Rahimpour, A. Tiraferri, In situ Ag-MOF growth on pre-grafted zwitterions imparts outstanding antifouling properties to forward osmosis membranes, ACS Appl. Mater. Interfaces 12 (32) (2020) 36287–36300.
[18] M. Pejman, M.D. Firouzjaei, S.A. Aktij, P. Das, E. Zolghadr, H. Jafarian, A.A. Shamsabadi, M. Elliott, M.R. Esfahani, M. Sangermano, Improved antifouling and antibacterial properties of forward osmosis membranes through surface modification with zwitterions and silver-based metal organic frameworks, J. Membr. Sci. 611 (2020) 118352.
[19] V. Anand Ganesh, B. Kundukad, D. Cheng, S. Radhakrishnan, S. Ramakrishna, K.J. Van Vliet, Engineering silver-zwitterionic composite nanofiber membrane for bacterial fouling resistance, J. Appl. Polym. Sci. 136 (22) (2019) 47580.
[20] L. Han, Y.Z. Tan, C. Xu, T. Xiao, T.A. Trinh, J.W. Chew, Zwitterionic grafting of sulfobetaine methacrylate (SBMA) on hydrophobic PVDF membranes for enhanced anti-fouling and anti-wetting in the membrane distillation of oil emulsions, J. Membr. Sci. 588 (2019) 117196.
[21] C.-Y. Liu, C.-J. Huang, Functionalization of polydopamine via the aza-michael reaction for antimicrobial interfaces, Langmuir 32 (19) (2016) 5019–5028.
[22] G. Ye, J. Lee, F.o. Perreault, M. Elimelech, Controlled architecture of dual-functional block copolymer brushes on thin-film composite membranes for integrated “defending” and “attacking” strategies against biofouling, ACS Appl. Mater. Interfaces 7 (41) (2015) 23069–23079.
[23] M.L.M. Tirado, M. Bass, M. Piatkovsky, M. Ulbricht, M. Herzberg, V. Freger, Assessing biofouling resistance of a polyamide reverse osmosis membrane surface-modified with a zwitterionic polymer, J. Membr. Sci. 520 (2016) 490–498.
[24] C. Liu, A.F. Faria, J. Ma, M. Elimelech, Mitigation of biofilm development on thin-film composite membranes functionalized with zwitterionic polymers and silver nanoparticles, Environ. Sci. Technol. 51 (1) (2016) 182–191.
[25] R. Hu, G. Li, Y. Jiang, Y. Zhang, J.-J. Zou, L. Wang, X. Zhang, Silver–zwitterion organic–inorganic nanocomposite with antimicrobial and antiadhesive capabilities, Langmuir 29 (11) (2013) 3773–3779.
[26] J. Zhao, Y. Zhang, Y. Su, J. Liu, X. Zhao, J. Peng, Z. Jiang, Cross-linked bovine serum albumin composite membranes prepared by interfacial polymerization with stimuli-response properties, J. Membr. Sci. 445 (2013) 1–7.
[27] J. Quirós, K. Boltes, S. Aguado, R.G. de Villoria, J.J. Vilatela, R. Rosal, Antimicrobial metal–organic frameworks incorporated into electrospun fibers, Chem. Eng. J. 262 (2015) 189–197.
[28] S. Chao, X. Li, Y. Li, Y. Wang, C. Wang, Preparation of polydopamine-modified zeolitic imidazolate framework-8 functionalized electrospun fibers for efficient removal of tetracycline, J. Colloid Interface Sci. 552 (2019) 506–516.
[29] M. Mozafari, S.F. Seyedpour, S.K. Salestan, A. Rahimpour, A.A. Shamsabadi, M.D. Firouzjaei, M.R. Esfahani, A. Tiraferri, H. Mohsenian, M. Sangermano, Facile Cu-BTC surface modification of thin chitosan film coated polyethersulfone membranes with improved antifouling properties for sustainable removal of manganese, J. Membr. Sci. 588 (2019) 117200.
[30] S.-W. Lv, J.-M. Liu, Z.-H. Wang, H. Ma, C.-Y. Li, N. Zhao, S. Wang, Recent advances on porous organic frameworks for the adsorptive removal of hazardous materials, J. Environ. Sci. (China) 80 (2019) 169–185.
[31] Z. Hasan, S.H. Jhung, Removal of hazardous organics from water using metal-organic frameworks (MOFs): plausible mechanisms for selective adsorptions, J. Hazard Mater. 283 (2015) 329–339.
[32] X. Li, W. Ma, H. Li, Y. Bai, H. Liu, Metal-organic frameworks as advanced sorbents in sample preparation for small organic analytes, Coord. Chem. Rev. 397 (2019) 1–13.
[33] N. Bazrafshan, M. Dadashi Firouzjaei, M. Elliott, A. Moradkhani, A. Rahimpour, Preparation and modification of low-fouling ultrafiltration membranes for cheese whey treatment by membrane bioreactor, Case Studies in Chemical and Environmental Engineering 4 (2021) 100137.
[34] A. Rahimpour, S.F. Seyedpour, S. Aghapour Aktij, M. Dadashi Firouzjaei, A. Zirehpour, A. Arabi Shamsabadi, S. Khoshhal Salestan, M. Jabbari, M. Soroush, Simultaneous improvement of antimicrobial, antifouling, and transport properties of forward osmosis membranes with immobilized highly-compatible polyrhodanine nanoparticles, Environ. Sci. Technol. 52 (2018) 5246–5258.
[35] Y.S. Li, H. Bux, A. Feldhoff, G.L. Li, W.S. Yang, J. Caro, Controllable synthesis of metal–organic frameworks: from MOF nanorods to oriented MOF membranes, Adv. Mater. 22 (30) (2010) 3322–3326.

[36] Y.S. Li, F.Y. Liang, H. Bux, A. Feldhoff, W.S. Yang, J. Caro, Molecular sieve membrane: supported metal–organic framework with high hydrogen selectivity, Angew. Chem. 122 (3) (2010) 558–561.
[37] M. Mazani, S. Aghapour Aktij, A. Rahimpour, N. Tavajohi Hassan Kiadeh, Cu-BTC metal– organic framework modified membranes for landfill leachate treatment, Water 12 (1) (2019) 91.
[38] A. Tiraferri, Y. Kang, E.P. Giannelis, M. Elimelech, Superhydrophilic thin-film composite forward osmosis membranes for organic fouling control: fouling behavior and antifouling mechanisms, Environ. Sci. Technol. 46 (20) (2012) 11135–11144.
[39] B. Yu, G. Ye, J. Chen, S. Ma, Membrane-supported 1D MOF hollow superstructure array prepared by polydopamine-regulated contra-diffusion synthesis for uranium entrapment, Environ. Pollut. 253 (2019) 39–48.
[40] H. Lee, S.M. Dellatore, W.M. Miller, P.B. Messersmith, Mussel-inspired surface chemistry for multifunctional coatings, Science 318 (5849) (2007) 426–430.
[41] J. Ren, P. Han, H. Wei, L. Jia, Fouling-resistant behavior of silver nanoparticle-modified surfaces against the bioadhesion of microalgae, ACS Appl. Mater. Interfaces 6 (6) (2014) 3829–3838.
[42] J. Ryu, S.H. Ku, H. Lee, C.B. Park, Mussel-inspired polydopamine coating as a universal route to hydroxyapatite crystallization, Adv. Funct. Mater. 20 (13) (2010) 2132–2139.
[43] W.O. Yah, H. Xu, H. Soejima, W. Ma, Y. Lvov, A. Takahara, Biomimetic dopamine derivative for selective polymer modification of halloysite nanotube lumen, J. Am. Chem. Soc. 134 (29) (2012) 12134–12137.
[44] M. Lee, S.H. Ku, J. Ryu, C.B. Park, Mussel-inspired functionalization of carbon nanotubes for hydroxyapatite mineralization, J. Mater. Chem. 20 (40) (2010) 8848–8853.
[45] J. Zhu, S. Yuan, A. Uliana, J. Hou, J. Li, X. Li, M. Tian, Y. Chen, A. Volodin, B. Van der Bruggen, High-flux thin film composite membranes for nanofiltration mediated by a rapid co-deposition of polydopamine/piperazine, J. Membr. Sci. 554 (2018) 97–108.
[46] X. Ruan, X. Zhang, Z. Zhou, X. Jiang, Y. Dai, X. Yan, G. He, ZIF-8 heterogeneous nucleation and growth mechanism on Zn (II)-doped polydopamine for composite membrane fabrication, Separ. Purif. Technol. 214 (2019) 95–103.
[47] Z. Liu, Y. Hu, Sustainable antibiofouling properties of thin film composite forward osmosis membrane with rechargeable silver nanoparticles loading, ACS Appl. Mater. Interfaces 8 (33) (2016) 21666–21673.
[48] S.F. Seyedpour, A. Rahimpour, G. Najafpour, Facile in-situ assembly of silver-based MOFs to surface functionalization of TFC membrane: a novel approach toward long-lasting biofouling mitigation, J. Membr. Sci. 573 (2019) 257–269.
[49] X. Wei, Z. Wang, J. Wang, S. Wang, A novel method of surface modification to polysulfone ultrafiltration membrane by preadsorption of citric acid or sodium bisulfite, Memb. Water Treat 3 (2012) 35–49.
[50] M. Ghanbari, D. Emadzadeh, W. Lau, T. Matsuura, A. Ismail, Synthesis and characterization of novel thin film nanocomposite reverse osmosis membranes with improved organic fouling properties for water desalination, RSC Adv. 5 (27) (2015) 21268–21276.
[51] A. Rahimpour, M. Jahanshahi, A. Mollahosseini, B. Rajaeian, Structural and performance properties of UV-assisted TiO 2 deposited nano-composite PVDF/SPES membranes, Desalination 285 (2012) 31–38.
[52] T.R. Van Assche, T. Duerinck, J.J. Gutierrez Sevillano, S. Calero, G.V. Baron, J.F. Denayer, High adsorption capacities and two-step adsorption of polar adsorbates on copper–benzene-1, 3, 5-tricarboxylate metal–organic framework, J. Phys. Chem. C 117 (35) (2013) 18100–18111.
[53] X.-p. Wang, J. Hou, F.-s. Chen, X.-m. Meng, In-situ growth of metal-organic framework film on a polydopamine-modified flexible substrate for antibacterial and forward osmosis membranes, Separ. Purif. Technol. 236 (2020) 116239.
[54] Y.-T. Zhao, L.-Q. Yu, X. Xia, X.-Y. Yang, W. Hu, Y.-K. Lv, Evaluation of the adsorption and desorption properties of zeolitic imidazolate framework-7 for volatile organic compounds through thermal desorption-gas chromatography, Anal. Methods 10 (40) (2018) 4894–4901.
[55] S.F. Seyedpour, A. Arabi Shamsabadi, S. Khoshhal Salestan, M. Dadashi Firouzjaei, M. Sharifian Gh, A. Rahimpour, F. Akbari Afkhami, M.r. Shirzad Kebria, M.A. Elliott, A. Tiraferri, Tailoring the biocidal activity of novel silver-based metal azolate frameworks, ACS Sustain. Chem. Eng. (2020).
[56] A. Kołodziejczak-Radzimska, E. Markiewicz, T. Jesionowski, Structural characterisation of ZnO particles obtained by the emulsion precipitation method, J. Nanomater. 2012 (2012) 1–9.
[57] A.A. Shah, Y.H. Cho, H.-g. Choi, S.-E. Nam, J.F. Kim, Y. Kim, Y.-I. Park, H. Park, Facile integration of halloysite nanotubes with bioadhesive as highly permeable interlayer in forward osmosis membranes, J. Ind. Eng. Chem. 73 (2019) 276–285.
[58] M. Li, P. Sun, Q. Wu, D. Liu, L. Zhou, Core–shell magnetic metal–organic framework molecularly imprinted nanospheres for specific adsorption of tetrabromobisphenol A from water, Environ. Sci.: Nano 5 (11) (2018) 2651–2662.
[59] H. Ang, L. Hong, Polycationic polymer-regulated assembling of 2D MOF nanosheets for high-performance nanofiltration, ACS Appl. Mater. Interfaces 9 (33) (2017) 28079–28088.
[60] N. Shahkaramipour, S.N. Ramanan, D. Fister, E. Park, S.R. Venna, H. Sun, C. Cheng, H. Lin, Facile grafting of zwitterions onto the membrane surface to enhance antifouling properties for wastewater reuse, Ind. Eng. Chem. Res. 56 (32) (2017) 9202–9212.
[61] K. Chen, K. Xie, Q. Long, L. Deng, Z. Fu, H. Xiao, L. Xie, Fabrication of core–shell Ag@ pDA@ HAp nanoparticles with the ability for controlled release of Ag+ and superior hemocompatibility, RSC Adv. 7 (47) (2017) 29368–29377.
[62] S. Zhao, Z. Wang, A loose nano-filtration membrane prepared by coating HPAN UF membrane with modified PEI for dye reuse and desalination, J. Membr. Sci. 524 (2017) 214–224.
[63] S. Kundu, B. Malik, D.K. Pattanayak, V.K. Pillai, Effect of dimensionality and doping in Quasi-"one-dimensional (1-D)" nitrogen-doped graphene nanoribbons on the oxygen reduction reaction, ACS Appl. Mater. Interfaces 9 (44) (2017) 38409–38418.
[64] Y. Li, X. Cai, S. Chen, H. Zhang, K.H. Zhang, J. Hong, B. Chen, D.H. Kuo, W. Wang, Highly dispersed metal carbide on ZIF-derived pyridinic-N-doped carbon for CO2 enrichment and selective hydrogenation, ChemSusChem 11 (6) (2018) 1040–1047.
[65] J. Xing, Q. Wang, T. He, Z. Zhou, D. Chen, X. Yi, Z. Wang, R. Wang, G. Tan, P. Yu, Polydopamine-Assisted immobilization of copper ions onto hemodialysis membranes for antimicrobial, ACS Applied Bio Materials 1 (5) (2018) 1236–1243.
[66] C.Y. Tang, Y.-N. Kwon, J.O. Leckie, Effect of membrane chemistry and coating layer on physiochemical properties of thin film composite polyamide RO and NF membranes: II. Membrane physiochemical properties and their dependence on polyamide and coating layers, Desalination 242 (1–3) (2009) 168–182.
[67] S. Xia, L. Yao, Y. Zhao, N. Li, Y. Zheng, Preparation of graphene oxide modified polyamide thin film composite membranes with improved hydrophilicity for natural organic matter removal, Chem. Eng. J. 280 (2015) 720–727.
[68] Q. Gu, T.C.A. Ng, W. Zang, L. Zhang, Z. Lyu, Z. Zhang, H.Y. Ng, J. Wang, Surface engineered alumina microfiltration membranes based on rationally constructed core-shell particles, J. Eur. Ceram. Soc. 40 (15) (2020) 5951–5958.
[69] Q. Gu, T.C.A. Ng, I. Zain, X. Liu, L. Zhang, Z. Zhang, Z. Lyu, Z. He, H.Y. Ng, J. Wang, Chemical-grafting of graphene oxide quantum dots (GOQDs) onto ceramic microfiltration membranes for enhanced water permeability and anti-organic fouling potential, Appl. Surf. Sci. 502 (2020) 144128.
[70] Q. Gu, H.Y. Ng, D. Zhao, J. Wang, Metal–Organic Frameworks (MOFs)-boosted filtration membrane technology for water sustainability, Apl. Mater. 8 (4) (2020), 040902.
[71] G.-d. Kang, Y.-m.J.W.r. Cao, in: Development of Antifouling Reverse Osmosis Membranes for Water Treatment: a Review, vol. 46, 2012, pp. 584–600, 3.
[72] M. Asadollahi, D. Bastani, S.A. Musavi, Enhancement of surface properties and performance of reverse osmosis membranes after surface modification: a review, Desalination 420 (2017) 330–383.
[73] B. Van der Bruggen, M. Mänttäri, M. Nyström, Drawbacks of applying nanofiltration and how to avoid them: a review, Separ. Purif. Technol. 63 (2) (2008) 251–263.
[74] A. Al-Amoudi, R.W. Lovitt, Fouling strategies and the cleaning system of NF membranes and factors affecting cleaning efficiency, J. Membr. Sci. 303 (1–2) (2007) 4–28.
[75] J. Liu, H. Xu, X. Tang, J. Xu, Z. Jin, H. Li, S. Wang, J. Gou, X. Jin, Simple and tunable surface coatings via polydopamine for modulating pharmacokinetics, cell uptake and biodistribution of polymeric nanoparticles, RSC Adv. 7 (26) (2017) 15864–15876.
[76] R. Tejido-Rastrilla, S. Ferraris, W.H. Goldmann, A. Grünewald, R. Detsch, G. Baldi, S. Spriano, A.R. Boccaccini, Studies on cell compatibility, antibacterial behavior, and zeta potential of Ag-containing polydopamine-coated bioactive glass-ceramic, Materials 12 (3) (2019) 500.
[77] J. Zhu, M. Tian, J. Hou, J. Wang, J. Lin, Y. Zhang, J. Liu, B. Van der Bruggen, Surface zwitterionic functionalized graphene oxide for a novel loose nanofiltration membrane, J. Mater. Chem. 4 (5) (2016) 1980–1990.
[78] J.D. Bryers, Biofilms and the technological implications of microbial cell adhesion, Colloids Surf. B Biointerfaces 2 (1–3) (1994) 9–23.
[79] S. Novak, U. Maver, Š. Peternel, P. Venturini, M. Bele, M. Gaberščček, Electrophoretic deposition as a tool for separation of protein inclusion bodies from host bacteria in suspension, Colloids Surf. A Physicochem. Eng. Asp. 340 (1–3) (2009) 155–160.
[80] H. Schwegmann, A.J. Feitz, F.H. Frimmel, Influence of the zeta potential on the sorption and toxicity of iron oxide nanoparticles on S. cerevisiae and E. coli, J. Colloid Interface Sci. 347 (1) (2010) 43–48.
[81] J. Li, J.-L. Gong, G.-M. Zeng, P. Zhang, B. Song, W.-C. Cao, S.-Y. Fang, S.-Y. Huan, J. Ye, The performance of UiO-66-NH2/graphene oxide (GO) composite membrane for removal of differently charged mixed dyes, Chemosphere 237 (2019) 124517.
[82] J. Fu, Z. Chen, M. Wang, S. Liu, J. Zhang, J. Zhang, R. Han, Q. Xu, Adsorption of methylene blue by a high-efficiency adsorbent (polydopamine microspheres): kinetics, isotherm, thermodynamics and mechanism analysis, Chem. Eng. J. 259 (2015) 53–61.
[83] M. Kadhom, N. Albayati, H. Alalwan, M. Al-Furaiji, Removal of dyes by agricultural waste, Sustainable Chemistry and Pharmacy 16 (2020) 100259.
[84] S. Krishnan, C.J. Weinman, C.K. Ober, Advances in polymers for anti-biofouling surfaces, J. Mater. Chem. 18 (29) (2008) 3405–3413.
[85] L. Shen, X. Zhang, J. Zuo, Y. Wang, Performance enhancement of TFC FO membranes with polyethyleneimine modification and post-treatment, J. Membr. Sci. 534 (2017) 46–58.
[86] Y. Zhang, J. Le Li, T. Cai, Z.L. Cheng, X. Li, T.-S. Chung, Sulfonated hyperbranched polyglycerol grafted membranes with antifouling properties for

sustainable osmotic power generation using municipal wastewater, J. Membr. Sci. 563 (2018) 521–530.
[87] R.R. Choudhury, J.M. Gohil, S. Mohanty, S.K. Nayak, Antifouling, fouling release and antimicrobial materials for surface modification of reverse osmosis and nanofiltration membranes, J. Mater. Chem. 6 (2) (2018) 313–333.
[88] M.D. Firouzjaei, A.A. Shamsabadi, M. Sharifian Gh, A. Rahimpour, M. Soroush, A novel nanocomposite with superior antibacterial activity: a silver-based metal organic framework embellished with graphene oxide, Adv. Mater. Interfac. 5 (11) (2018) 1701365.
[89] Y. Wu, M. Gao, W. Chen, Z. Lü, S. Yu, M. Liu, C. Gao, Efficient removal of anionic dye by constructing thin-film composite membrane with high perm-selectivity and improved anti-dye-deposition property, Desalination 476 (2020) 114228.
[90] P. Zhao, R. Li, W. Wu, J. Wang, J. Liu, Y. Zhang, In-situ growth of polyvinylpyrrolidone modified Zr-MOFs thin-film nanocomposite (TFN) for efficient dyes removal, Compos. B Eng. 176 (2019) 107208.
[91] J. Ding, H. Wu, P. Wu, Development of nanofiltration membranes using mussel-inspired sulfonated dopamine for interfacial polymerization, J. Membr. Sci. 598 (2020) 117658.
[92] X. Liang, P. Wang, J. Wang, Y. Zhang, W. Wu, J. Liu, B. Van der Bruggen, Zwitterionic functionalized MoS2 nanosheets for a novel composite membrane with effective salt/dye separation performance, J. Membr. Sci. 573 (2019) 270–279.
[93] Y.-H. Chiao, S.-T. Chen, M.B.M. Yap Ang, T. Patra, D.A. Castilla-Casadiego, R. Fan, J. Almodovar, W.-S. Hung, S.R. Wickramasinghe, High-performance Polyacrylic acid-grafted PVDF nanofiltration membrane with good antifouling property for the textile industry, Polymers 12 (11) (2020) 2443.
[94] J. Li, S. Yuan, J. Zhu, B. Van der Bruggen, High-flux, antibacterial composite membranes via polydopamine-assisted PEI-TiO2/Ag modification for dye removal, Chem. Eng. J. 373 (2019) 275–284.